JACS
JOURNAL OF THE AMERICAN CHEMICAL SOCIETY
Article
pubs.acs.org/JACS

Time-Resolved Fluorescence Spectroscopy Measures Clustering and Mobility of a G Protein-Coupled Receptor Opsin in Live Cell Membranes

William D. Comar,[§,‡] Sarah M. Schubert,[§,†,‡] Beata Jastrzebska,[∥] Krzysztof Palczewski,[∥] and Adam W. Smith*[,§]

[§]The University of Akron Department of Chemistry, 190 Buchtel Common, Akron, Ohio 44303-3601, United States
[∥]Department of Pharmacology, School of Medicine, Case Western Reserve University, 2109 Adelbert Road, Cleveland, Ohio 44106-4965, United States

ABSTRACT: Determining membrane protein quaternary structure is extremely challenging, especially in live cell membranes. We measured the oligomerization of opsin, a prototypical G protein-coupled receptor with pulsed-interleaved excitation fluorescence cross-correlation spectroscopy (PIE-FCCS). Individual cell measurements revealed that opsin is predominantly organized into dimeric clusters. At low concentrations, we observed that the population of oligomers increased linearly with the square of the individual monomer populations. This finding supports a monomer−dimer equilibrium and provides an experimental measurement of the equilibrium constant.

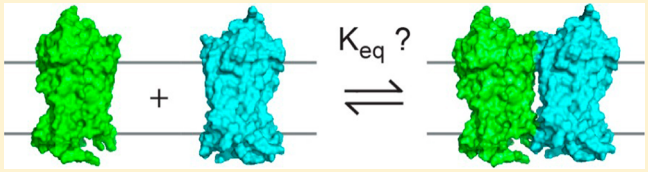

INTRODUCTION

Membrane receptor dimerization and assembly is essential in many cell-signaling pathways, but remains controversial for many others. The reason for the controversy is the complex nature of the plasma membrane and the lack of tools to probe these structures in situ. G protein-coupled receptor (GPCR) oligomerization, for example, remains controversial despite numerous investigations.[1] The prevalence and physiological role of GPCR oligomers is of central concern because GPCRs are the largest family of membrane proteins in the mammalian genome and a large fraction of drugs target these receptors.[2]

Here we describe our work with a time-resolved fluorescence technique, pulsed-interleaved excitation fluorescence cross-correlation spectroscopy (PIE-FCCS), to study opsin oligomerization in a live cell membrane. PIE-FCCS translates fluctuations in fluorescence signal (arising mainly from diffusion) into information about a protein's mobility and concentration. With PIE-FCCS it is possible to measure correlated movements of proteins such that the population of stable complexes can be quantified with high accuracy. We observed that opsin, a prototypical GPCR, is organized into dimers. At low concentrations we found a linear increase of the dimer population with the square of monomer concentration, from which we obtained an equilibrium constant for the dimerization reaction.

Rhodopsin (opsin +11-*cis*-retinal) is the light-sensitive protein at the heart of scotopic vision and the first GPCR to be crystallized and structurally resolved.[3] In the retina, rhodopsin is highly concentrated in rod cell outer segment (ROS) membranes (~24 000 molecules/μm^2).[4] Early experiments indicated that it was rotationally and translationally mobile in those membranes,[5] which led to the conclusion that rhodopsin is monomeric. In support of this conclusion, single protein activity assays showed that monomeric rhodopsin could enable signal transduction.[6] Alternatively, there is a large body of biophysical work showing that rhodopsin is dimerized in native membranes. Evidence for rhodopsin dimers ranges from detergent-stabilized complexes to optical imaging and atomic force microscopy of isolated ROS membranes.[7] Still lacking from this work is a full characterization of the thermodynamics of opsin dimerization in native membranes.

Our solution to this problem is a time-resolved fluorescence technique, PIE-FCCS,[8] which quantifies the population of receptors that codiffuse as homo-oligomers while simultaneously quantifying the total population of receptors. This live-cell compatible technique has been used to resolve the mechanism of epidermal growth factor activation and inhibition,[9] as well as the organizational principles affecting lipid-anchored proteins.[10] One advantage of PIE-FCCS is that it relies on receptors diffusing in and out of a small area defined by a laser focus. This makes it possible to measure the mobility of the receptors at higher densities and with a sampling rate superior to single-molecule tracking. It also serves as a spatiotemporal filter, which excludes large immobile aggregates and internal organelles from the analysis. This removes some of the artifacts that can result in overestimation of the dimer fraction by methods based on resonant energy transfer.

Received: February 24, 2014
Published: May 15, 2014

 © 2014 American Chemical Society dx.doi.org/10.1021/ja501948w | *J. Am. Chem. Soc.* 2014, 136, 8342−8349

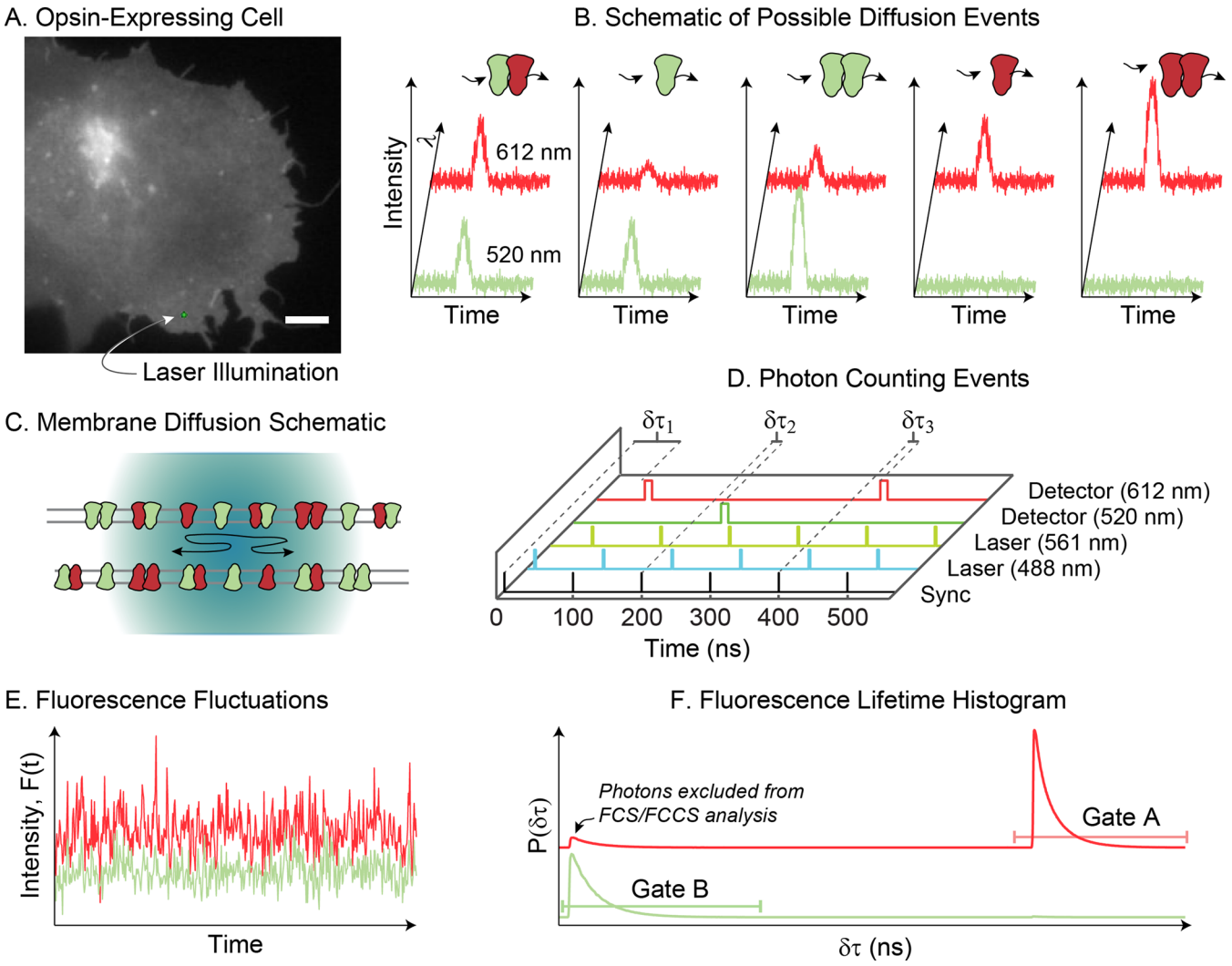

Figure 1. PIE-FCCS schematic. (A) An epi-fluorescence image of an opsin-eGFP-expressing Cos-7 cell is merged with an image of fluorescence excited by the laser used for PIE-FCCS (scale bar = 5 μm). The arrow points to the laser illumination area shown in green, which has a radius of ~220 nm. (B) Several possible diffusing species are diagrammed to show their respective contributions to the total fluorescence signal. The red/green dimer diffusing through the laser focus leads to a spike of intensity in the 520 and 612 nm detector channels. Green monomers or dimers show a spike of intensity in the green channel proportional to the number of receptors, as well as some intensity in the red channel. This spectral bleed-through is removed with PIE using the time gating shown in panels D and F. Red monomers and dimers display essentially no bleed-through to the 520 nm detector. (C) Schematic showing that the laser excites fluorescence in the basal and apical membranes of Cos-7 cells and that on average there are many receptors diffusing in and out of the laser focus. (D) Pulse diagram showing the interleaving of the 488 and 561 nm lasers. Each photon detection event is time-tagged to a sync pulse (from laser system), which allows for the assignment of that photon to either 488 or 561 nm excitation. (E) For a sample with more than one fluorescent species, multiple overlapping diffusion events cause the fluctuations, but the correlation analysis described in the Experimental Section can quantify the concentration and mobility of the molecules in the signal. (F) A lifetime histogram shows the number of photon detection events occurring at each value of $\delta\tau$. This information is used to select the time gates for the red and green species (Gates A and B) and rejects photons arising from spectral bleed-through or cross-talk from the correlation analysis.

RESULTS AND DISCUSSION

In this study we measured opsin oligomerization in a live cell membrane under physiological conditions. Because of the high density of opsin in native ROS membranes, we expressed the receptor in cultured COS-7 cells. This cellular environment served as a native-like membrane system, where the density of the receptor can be passively varied through transient transfection. For the data shown here, we observed opsin at expression densities ranging from 100 to 2000 molecules/μm^2.

The apparatus used for the PIE-FCCS experiments is described in detail in the Experimental Section. It essentially consisted of dual-laser point excitation and dual-band confocal detection with single-photon avalanche photodiodes. The laser system was a white-light picosecond-pulsed fiber laser, from which two narrow bands were selected (488 ± 2 and 561 ± 2 nm) and temporally separated by a fixed fiber delay. The temporal offset interleaves the two pulse trains in time so that any fluorophore excited by one pulse (e.g., 488 nm) decays before the next pulse arrives (e.g., 561 nm). This strategy sorts the photons into four data channels: the product of two time gates and two color channels (see Figure 1).

In PIE-FCCS, photons arriving during the 488 nm pulse time gate and the green (520/44 nm) color channel were used to calculate the green (eGFP) autocorrelation curve, whereas photons arriving during the 561 nm pulse time gate and the red (612/69 nm) color channel were used to calculate the red

dx.doi.org/10.1021/ja501948w | J. Am. Chem. Soc. 2014, 136, 8342−8349

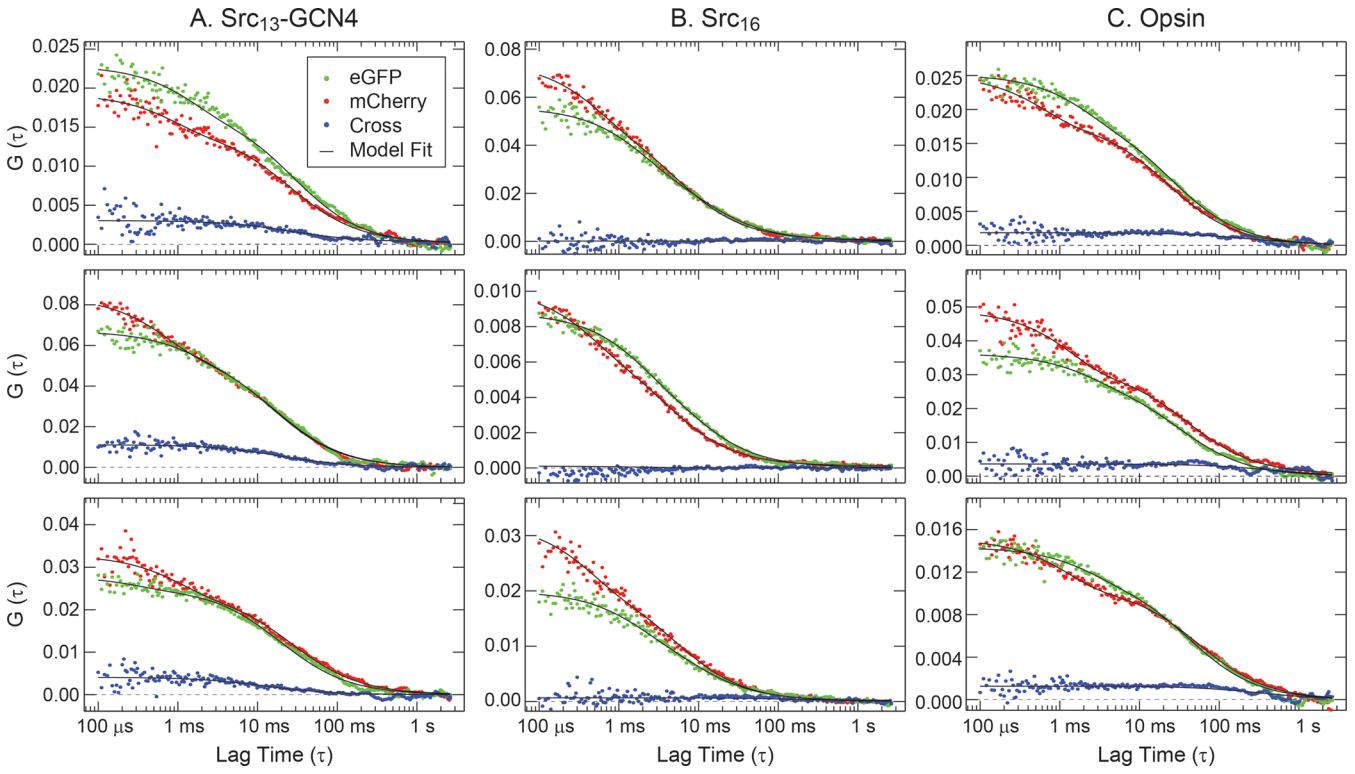

Figure 2. Representative FCCS data. FCCS data are shown for (A) Src_{13}-GCN4, (B) Src_{16}, and (C) opsin expressed in Cos-7 cells. In each plot, colored dots are the measured data points, whereas the solid black lines indicate the fitted functions (defined in the Experimental Section). Red dots are the FCS data for the mCherry fusion protein, $G_R(\tau)$, green dots are the FCS data for the eGFP fusion, $G_G(\tau)$, and blues dots are the FCCS data, $G_X(\tau)$. Amplitude data report directly on the concentration of diffusing species through the relationship $G_i(0) = 1/\langle N_i \rangle$ and are used to calculate f_c as shown in the text. In each plot, a horizontal dashed line marks the zero value for comparison with the cross-correlation amplitude, $G_X(0)$.

(mCherry) autocorrelation curve. The same data were used to calculate the cross-correlation spectrum, resulting in freedom from cross-talk (488 nm light exciting mCherry) and spectral bleed-through (eGFP emission in the red channel).[9]

Example PIE-FCCS data are shown for three dual-expression constructs. The first (Figure 2A) is a lipid-anchored peptide derived from cSrc fused to the GCN4 α-helical dimerization motif[11] and a C-terminal eGFP or mCherry fluorescent protein, Src_{13}-GCN4-eGFP/mCherry. The second (Figure 2B) is the cSrc derived peptide fused directly to the fluorescent protein,[12] Src_{16}-eGFP/mCherry. The Src_{16} and Src_{13}-GCN4 constructs were identical to those used in a previous publication where they served as a negative and positive control, respectively, for cross-correlation in the experiment (named Myr-FP and Myr-GCN4-ICM in ref 9). The fact that we found zero cross-correlation for Src_{16} demonstrates that PIE effectively removed artifacts that would have led to false-positive cross-correlation and that the fluorescent proteins themselves did not drive dimerization. The Src_{13}-GCN4 data show the upper limit for a strongly dimerized system due to protein dark states[13] and the presence of dimers with identical fluorescent protein tags (see Figure 1B). Finally, Figure 2C shows example PIE-FCCS data for opsin with C-terminal eGFP or mCherry.

To quantify the mobility and clustering of opsin compared to the control proteins, PIE-FCCS data were fit to a simple 2D diffusion model (see Experimental Section). Autocorrelation spectra were fit to a single-component diffusion model with triplet relaxation. Cross-correlation spectra were fit to a single diffusing species model without triplet relaxation. Meaningful parameters obtained from these fits were (i) the number of diffusing species in the laser focus, (ii) the fraction of molecules diffusing as a complex, and (iii) the mobility of the receptors. Each of these parameters is discussed later. Fluorescence correlation spectra (FCS) at early time points are inversely proportional to the number of diffusing species in the laser focus ($G_i(\tau) = 1/\langle N_i \rangle$). The fraction of receptors incorporated into clusters, f_c, was calculated by taking the ratio of the number of red or green diffusing species $N_{R\ or\ G}$ and the number of codiffusing species N_X:[9,14]

$$f_c = \frac{N_X}{N_{RorG}}$$

Calculated in this way, f_c represents the fraction of receptors labeled with eGFP that codiffuse with receptors labeled with mCherry (or vice versa).

To characterize the extent of oligomerization for each construct, we measured multiple cells in four (or more) independent experiments. Figure 2 summarizes the results of these measurements by plotting f_c values along the vertical axis and spreading the values along the x-axis in vertical bin values of 0.05. The Src_{13}-GCN4 data showed a median f_c value of 0.23 and a mean of 0.25 ± 0.10. The spread in f_c values reflects cell-to-cell variability and weak density dependence at low concentrations. The mean f_c of 0.25 is the maximum correlation one would expect based on the large dark state population of mCherry[13] and the statistics of dimerization between eGFP and mCherry labeled proteins, eGFP/eGFP:eGFP/mCherry:mCherry/mCherry (1:2:1).[9,13] The Src_{16} data showed f_c values that were tightly clustered near zero, with a median value of 0.016 and a mean of 0.025 ± 0.022, consistent with previous measurements.[9]

dx.doi.org/10.1021/ja501948w | J. Am. Chem. Soc. 2014, 136, 8342−8349

For the opsin protein, 79 individual cells were measured, and the resulting f_c values are shown in Figure 2. Over 90% of the cells displayed nonzero cross-correlation ($f_c > 0.05$), indicating that opsin is significantly distributed into oligomers. The values of f_c were spread over a wide range with a median value of 0.10 and a mean/standard deviation of 0.12 ± 0.08. The mean f_c value was half that of the positive control, indicating significant yet incomplete oligomerization. The spread in f_c values for opsin reflects cell-to-cell variability as well as a density dependence that will be addressed below.

We also measured the cross-correlation of opsin with another class-A GPCR, the dopamine D2 receptor (D2R). Opsin and dopamine receptors play disparate physiological roles but share structural similarities that could potentially lead to clustering in the plasma membrane. Testing for specificity is one way to determine if opsin oligomerization is specific for homo-oligomerization or if it is a nonspecific property of GPCRs. The distribution of cross-correlation for the opsin−D2R expressing cells in Figure 3 indicated that opsin−D2R oligomers were much less prevalent than opsin−opsin oligomers. The distribution of f_c values was similar to that for the Src_{16} monomer, but with a median value of 0.035 and a mean/standard deviation of 0.054 ± 0.054. This provides evidence that opsin homodimerization is specific and suggests that opsin oligomers are not passively formed by structural features shared with other Class A GPCRs.

The time decay of the correlation spectra reports directly on the mobility of the receptors and is sensitive to protein cluster size. Mobility alone cannot unambiguously distinguish oligomer size due to the unresolved relationship between protein size, oligomer state, and mobility in plasma membranes.[15] However, the diffusion coefficient can be extracted from the data for comparison among the proteins studied here and with previous literature values. To quantify mobility, we related the diffusion coefficient to the decay time of the FCS curves, τ_{Di}, and the radius, ω_0, of the lasers at the focus through the following equation:

$$D_{\text{eff}} = \sqrt{\frac{\omega_0^2}{4\tau_{Di}}}$$

Because there are likely to be other contributions to protein mobility besides pure Brownian motion, we refer to this as the effective diffusion coefficient, D_{eff}. In Figure 4, D_{eff} was calculated from the green autocorrelation data. The Src_{16} diffusion coefficient was nearly as high as that for free lipids in the plasma membrane,[16] consistent with a protein anchored to the membrane by a single acyl chain. The Src_{13}-GCN4 construct showed a much smaller diffusion coefficient, consistent with a dimer complex with a large effective radius in the membrane. Opsin diffusion was similar to the positive control and comparable to that of other GPCRs,[17] and the average $D_{\text{eff}} = 0.38 \pm 0.15$ for opsin is consistent with monomer and small oligomer diffusion.

One method to estimate the size of the opsin oligomers observed in the PIE-FCCS data is molecular brightness analysis. Molecular brightness quantifies the average number of photons emitted by each species as it enters and exits the laser focus. A similar method is the photon-counting histogram, which has been used to estimate the size of other GPCRs.[17a] FCS data encode this information as the ratio of the average number of molecules, N_i, divided by the photon count rate, or counts per second (cps_i). We refer to this ratio as the molecular brightness, indicated by the symbol η_i.

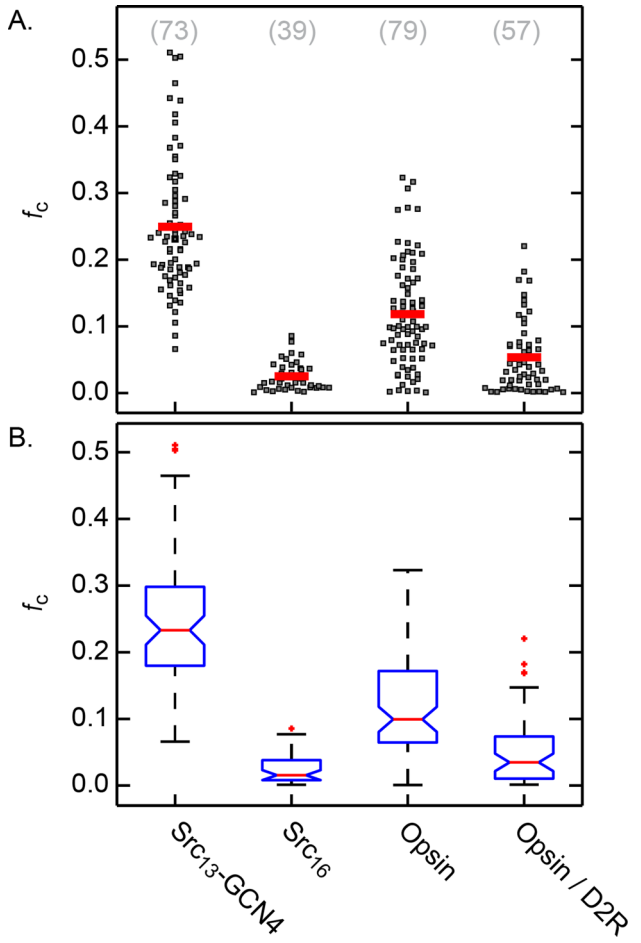

Figure 3. Summary of cross-correlation data. (A) The f_c value for each individual cell is plotted on the vertical axis and grouped by protein type. The spread in the horizontal dimension is proportional to the number of cells within 0.05 intervals of f_c. Numbers in parentheses at the top of the graph are the total number of data points or unique cells measured for each construct. The red line indicates the mean value of the distribution. (B) Box and whisker plots are shown for the identical data points in panel A. The red line is the median value. The blue boxes enclose the 25−75% percentile values, and the notches indicate the range over which two distributions are different to the 5% confidence level. Whiskers enclose the most extreme points not considered outliers and outliers are marked in red.

$$\eta_i = \frac{N_i}{\text{cps}_i}$$

We conducted brightness experiments in GFP-only expressing cells. Cells were otherwise treated and measured identically to the PIE-FCCS experiments discussed above. The FCS data are calculated and fit as described for the dual-color experiments, and the molecular brightness is calculated using the ratio above. In Figure 5 we see that the molecular brightness of Src_{16}-eGFP proteins is slightly more than half of the brightness of the Src_{13}-GCN4-eGFP proteins. The molecular brightness of opsin-eGFP is nearly identical to the monomer control, but with a larger spread in values indicative of a range of clustering. This is consistent with the distribution of f_c values shown in Figure 3 and indicates that opsin may be

dx.doi.org/10.1021/ja501948w | J. Am. Chem. Soc. 2014, 136, 8342−8349

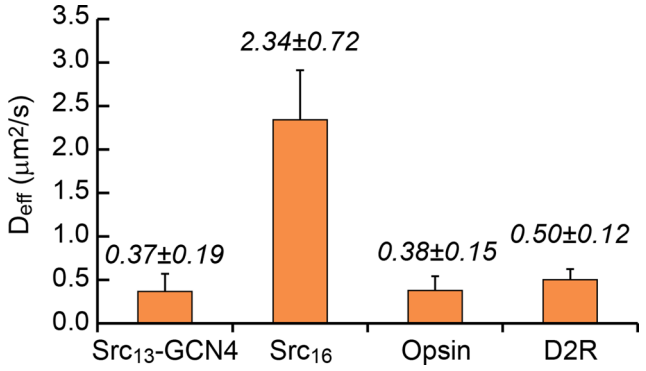

Figure 4. Mobility. The effective diffusion coefficient, D_{eff}, is shown for each of the indicated GFP-labeled protein species. The diffusion coefficients were calculated from the fit τ_D as indicated in the text. The column height is the mean value averaged over the same cell data as in Figure 3. Error bars indicate standard deviations. The means and standard deviations are also printed above each of the columns for clarity.

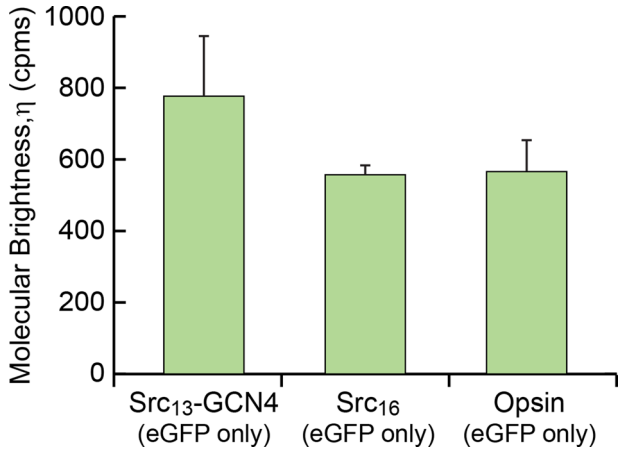

Figure 5. Molecular brightness. The molecular brightness for cells expressing Src_{16}-eGFP, Src_{13}-GCN4-eGFP, or opsin-eGFP was calculated from single-color FCS data as described in the text. Error bars indicate the standard deviation.

found as monomers and dimers, but higher-order oligomers are not likely to be present.

Another metric for determining the degree of opsin clustering is Förster resonance energy transfer (FRET). This has been used to quantify opsin dimerization in the past and could potentially be a factor in the present experiments.[7c,18] The data collected for the PIE-FCCS analysis was recorded in a time-correlated single-photon counting mode, so we could also construct lifetime histograms as described in Figure 1. In this way we experimentally measure the fluorescent lifetime of each protein construct. Fluorescent lifetimes are sensitive to the probe environment and are good indicators of resonant energy transfer. The eGFP and mCherry fluorophore labels in this study are not an ideal FRET pair but have been used in the past for FRET analyses.[19] Moreover, the lifetime FRET data serve as a quality control test for the PIE-FCCS results. This is because strong FRET could bias the FCCS data and the resulting f_c values.[8]

For the lifetime FRET analysis, we used the same photon data employed to calculate the PIE-FCCS data summarized in Figure 3. The lifetime histograms were binned at 32 ps intervals and fit to a single exponential curve convolved with the instrument response function. The lifetime fit results are shown in Figure 6A, where lifetime fit for each of the five 15-s

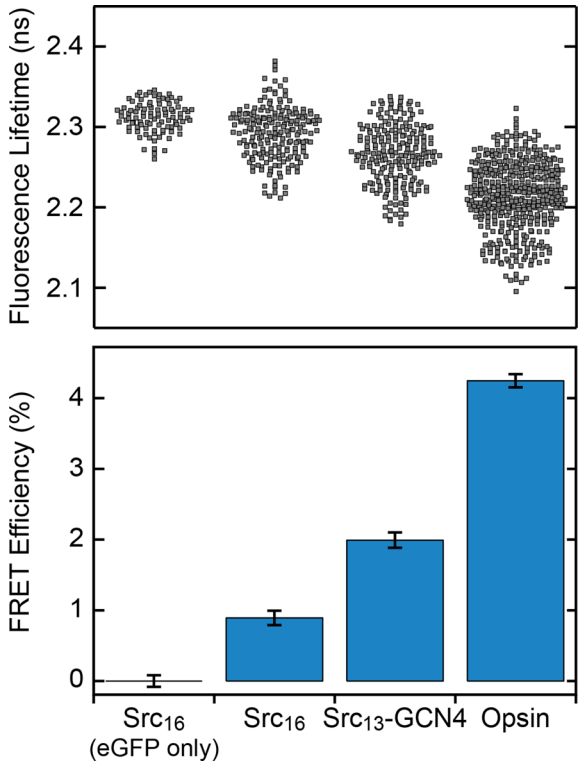

Figure 6. FRET analysis. (A) Scatter plot of fluorescence lifetimes fit as described in the text. Each data point is a 15-s measurement and each cell was measured five times. (B) Bar graph of average FRET efficiency calculated from the lifetimes as described in the text. Error bars indicate the standard errors of the mean.

measurements made per cell is displayed. The average lifetime of eGFP in cells expressing only Src_{16}-eGFP was used as the τ_0 value in the following equation to estimate the FRET efficiency, E_{FRET}.

$$E_{FRET} = 1 - \frac{\tau_A}{\tau_0}$$

Here, τ_A is the lifetime of the donor in the presence of the acceptor. Figure 6B shows the average FRET efficiency for each of the constructs. The Src_{16} data show a very low FRET efficiency, while the dimer shows only a small relative increase. This small FRET value for Src_{13}-GCN4 is likely due to the distance and orientation of the fluorophores in the dimer complex. This is because the fluorescent proteins are fused to the C-terminal tails of the EGFR kinase domain, which dimerize in a way that keeps the C-terminal labels several nanometers apart.[9,20] The opsin construct shows a modest FRET efficiency of 4.2 ± 0.1%. (Here and in Figure 6, the error is reported as the standard error of the mean.) The low value of FRET efficiency for each of the constructs shows that resonant energy transfer is not strongly influencing the PIE-FCCS data.[8]

The mobility, molecular brightness, and lifetime FRET data are consistent with opsin existing as monomers or small oligomers. From this, we hypothesize that, under the conditions of these experiments, opsin in the plasma membrane is in a monomer−dimer equilibrium, with no resolvable population of higher-order oligomers. To further test this hypothesis, we

dx.doi.org/10.1021/ja501948w | J. Am. Chem. Soc. 2014, 136, 8342−8349

returned to the cross-correlation data, where the distribution of f_c values provides a statistical overview of the extent of opsin dimerization in the plasma membrane. Buried in this analysis is the fact that, for each cell measured, PIE-FCCS quantifies f_c and the total number of diffusing species. If we posit a monomer−dimer equilibrium, then the PIE-FCCS data can be used to determine the concentration of monomer and dimer species in the membrane. The chemical reaction for dimerization can be written as

$$\text{opsin} + \text{opsin} \leftrightarrow \text{opsin}\cdot\text{opsin}$$

The equilibrium constant for this reaction is then given by

$$K_{eq} = \frac{[\text{opsin}\cdot\text{opsin}]}{[\text{opsin}]^2}$$

To determine K_{eq}, we plotted the individual cell data as the product of the eGFP- and mCherry-labeled monomer concentrations versus the concentration of dimers (Figure 7). At sufficiently low receptor concentrations, each of the scatter plots showed a linear trend, consistent with a monomer−dimer equilibrium.[14b]

As seen in Figure 7, the dimer concentrations of opsin and Src_{16} increased linearly up to 40 000 molecules$^2/\mu m^4$ or 200 molecules/μm^2. This linear relationship is consistent with our model and is evidence that opsin clustering is dominated by dimerization and not higher-order clustering in this range of concentrations. At higher concentrations the data were more scattered, indicative of either more complex diffusional behavior or larger noise in the FCCS measurements. For opsin, a linear fit to the data in Figure 7 gave a slope of $9.94 \pm 0.53 \times 10^{-4}$ (molecules/μm^2)$^{-1}$. Under the assumptions of the simple model above, the slope is equal to K_{eq} for the dimerization reaction. The K_{eq} value for opsin then could be compared to that of the monomer control, Src_{16}. Over the same range, the Src_{16} data were fit to a line with a slope of $1.08 \pm 0.19 \times 10^{-4}$ (molecules/μm^2)$^{-1}$, ~1 order of magnitude lower than that of opsin.

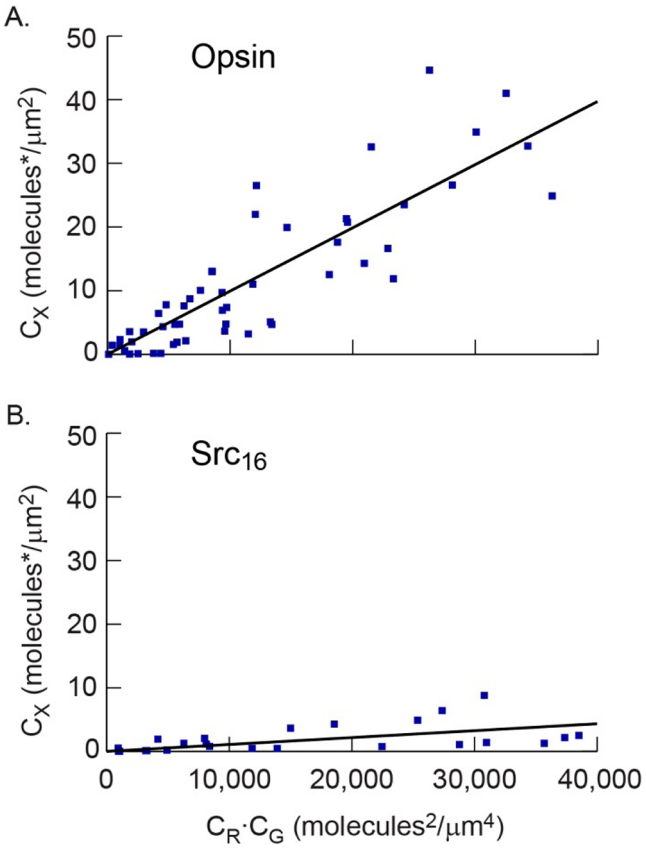

Figure 7. Dimerization equilibrium constants. Protein concentrations, C_i, were obtained from the model fits to the FCS data and the area of the laser focus. At low concentrations, plots reveal a linear increase in the dimeric species concentration, C_X, versus the product of the monomer species, C_R and C_G. The slope provides the equilibrium coefficient for each dimerization reaction.

The K_{eq} for dimerization, to our knowledge, has only been reported for one other GPCR, the *N*-formyl peptide receptor (FPR). Using single-molecule imaging at low receptor concentrations (<2.6 molecules/μm^2), the authors reported a 2-dimensional dimer dissociation constant of 3.6 molecules/μm^2.[21] This is more than 250 times smaller than the dissociation constant we measure for opsin (2D-K_D = $1/K_{eq}$ = 1 010 molecules/μm^2). This likely indicates a substantially different affinity for dimerization of these two receptors, but further work is needed to directly compare the two methods.

CONCLUSIONS

To understand the implications of the K_{eq} obtained from this analysis, it is useful to consider the fraction of proteins found in dimers at various concentrations in the membrane. First, based on the fit K_{eq} value above, the fraction of opsin proteins found in dimeric complexes would be 50% at a total opsin concentration of 1 006 molecules/μm^2. This is consistent with the opsin f_c distribution in Figure 3, which had a mean value one-half that of the positive control and was taken at a concentration range centered at 1 000 molecules/μm^2. At much higher concentrations, similar to those of rhodopsin found in ROS membrane disks (~24 000 molecules/μm^2), 87% of the total protein population would be found in a dimeric complex.

Within ROS membranes it is possible that further oligomerization of rhodopsin dimers could occur.[7a,b] There is also the possibility that the intradiscal domains of two rhodopsin molecules located on two facing layers of membrane on the same ROS disc could provide an additional stabilizing force, leading to further immobilization and self-aggregation of this receptor.[4] These organizational features could be essential for development of ROS structure. At the other end of this multistage equilibrium, a modest dimerization K_{eq} would allow the rhodopsin monomer to also be present in appreciable amounts.

We have shown that PIE-FCCS can resolve the concentration of dimeric opsin in the plasma membranes of live cells. From these results we calculated the equilibrium constant for opsin dimerization, which to date has not been reported. Our results show that PIE-FCCS provides a powerful platform to quantify membrane protein mobility and clustering. The method could greatly impact future studies of membrane receptor clustering, which is increasingly thought to influence cell communication.

EXPERIMENTAL SECTION

PIE-FCCS Instrument. Fluorescence imaging and spectroscopy measurements were made with a customized inverted microscope (Nikon Eclipse Ti, Toyko, Japan). For laser excitation we used the output of a continuum white light laser (SuperK NKT Photonics, Birkerød, Denmark) operating at 9.7 MHz with an internal pulse picker. Two excitation beams were selected from the parent

dx.doi.org/10.1021/ja501948w | J. Am. Chem. Soc. 2014, 136, 8342−8349

continuum beam with bandpass filters and then cleaned up with narrowband filters. The blue beam passed through a 488 nm filter with a 1.9 nm full width half max (fwhm) bandwidth (LL01-488-12.5, Semrock, Rochester, NY) whereas the green beam passed through a 561 nm filter with a 2.1 fwhm bandwidth (LL02-561-12.5, Semrock, Rochester, NY). For optimal mode overlap each beam was coupled to an identical core single mode optical fiber (QPMJ-3AF3U-488-3.5/125-3AS-18-1-SP and QPMJ-3AF3U-488-3.5/125-3AS-3-1-SP, OZ Optics, Ottawa, Ontario). The beams passed through fibers of different lengths (18 m for α_{488} and 3 m for α_{561}), to introduce a 50 ns delay between the two pulse trains for pulsed interleaved excitation (PIE). The two beams exited their respective fibers with identical coupling lenses and were overlapped with a 503 nm cutoff dichroic beam splitter (LM01-503-25, Semrock, Rochester, NY). The combined beam was then fed into the microscope using a laser filter cube (91032, Chroma Technology Corp., Bellows Falls, VT) with a two-color dichroic mirror and laser blocking filter (zt488/561rpc and zet488/561m, Chroma Technology Corp., Bellows Falls, VT). A 100X TIRF objective, NA 1.49 (Nikon Corp., Tokyo, Japan), was used to focus the excitation light on the sample and collect the emitted fluorescence.

For time-correlated single-photon counting, we employed a custom-built confocal detection unit with a 50 μm confocal pinhole (Thorlabs, Newton, NJ) placed at one of the output ports of the microscope. Light passing through the pinhole was collimated and then split with a 560 nm long-pass beam splitter (FF560-F,Di01-25x36, Semrock, Rochester, NY). Each beam then was focused to a single photon avalanche diode (SPAD) with a 50 μm active area, 30 ps timing resolution, and 25 dark counts per second (Micro Photon Devices, Bolzano, Italy). The red beam passed through a 612/69 nm filter (FF01-621/69-25, Semrock, Rochester, NY) and the green beam passed through a 520/44 nm filter (FF01-520/44-25, Semrock, Rochester, NY). The data were recorded with a four-channel-routed time-correlated single-photon counting (TCSPC) device (Picoharp 300, PicoQuant, Berlin, Germany).

To ensure maximal overlap between the 520 and 612 nm detection volumes, we regularly measured the cross-correlation of a 41 base pair DNA oligonucleotide with a TAMRA dye on the 5′ end and a 6-FAM dye on the 3′ end. With this control we measured an f_c of 0.80.

Cell Culture and Transfection. Mammalian cell culture and transfection was carried out with standard protocols. Cos-7 cells were cultured in Dulbecco's modified Eagle's medium (DMEM 1× + GlutaMAX, Life Technologies, Grand Island, NY) supplemented with 10% fetal bovine serum (FBS, Life Technologies) and 1% penicillin/streptomycin (BioReagent, Sigma-Aldrich). Cells were grown in 100 × 20 mm Petri dishes and split when they reached ∼95% confluency. Cells were passaged up to 7 times. Two to three days prior to imaging, cells were seeded into 35 × 10 mm uncoated glass bottom dishes with #1 coverslips (MatTek) and grown to 70−90% confluency before transfection. Cells were transfected 1 day prior to imaging with the Lipofectamine 2000 transfection reagent (Life Technologies) following the supplier's protocols. The media for transfected cells was changed from DMEM to Opti-MEM I media without phenol red (Life Technologies) prior to imaging.

Plasmids. The Src_{16}-eGFP/mCherry and Src_{13}-GCN4-eGFP/mCherry plasmids provided by Jay T. Groves (U.C. Berkeley) have been described previously.[9,10] The plasmid for the dopamine D2R measurements, pcDNA-D2s-L-Venus, was obtained from Addgene (Cambridge, MA) and used without modification. For construction of opsin-EGFP and opsin-mCherry, mouse opsin cDNA was amplified by PCR and EcoR1 and BamH1 restriction sites were introduced at the 5′- and 3′-ends, respectively, by using the following primers: for the opsin-EGFP construct, forward primer GTGGGGAATTCGCCATGAACGGGCACAGAGGG and reverse primer TCTGGGGATCCGGCTGGAGCCACCTGG; for opsin-mCherry construct, forward primer GTGGGGAATTCGCCATGAACGGCACAGAGGG and reverse primer TCTGGGGATCCCGGGCTGGAGCCACCTGG. Amplified DNA was cloned into pEGFP-N3 and pmCherry-N1 original vectors (Clontech, Mountain View, CA), respectively. The functional relevance of these fluorescent protein fusion constructs was demonstrated in previous work.[7c,18]

Data Collection and Analysis. Measurements were made on live cells maintained at 37 °C in a stage-top incubator (Chamlide IC, Quorum Technologies, Guelph, Ontario). For each measurement, laser powers were set to 800 nW (488 nm) and 1 μW (561 nm), measured before the light entered the microscope light path. During imaging, cells with similar expression levels of mCherry and eGFP fluorescence were selected and TCSPC data were collected at 5 × 15 s intervals for each cell.

The TCSPC data were processed by constructing a fluorescence intensity plot that contained the number of photons detected in sequential 10 μs bins. Data were time-gated to include only photons collected within 0.2 ns before and 70 ns after the 488 nm laser pulse arrival time for $F_G(t)$ and 0.2 ns before and 30 ns after the 561 nm laser pulse arrival time for $F_R(t)$. The autocorrelation curves were then calculated with a multiple tau algorithm used in previous publications,[9,10] which is numerically equivalent to the following expression:

$$G_i(\tau) = \frac{\langle \delta F_i(t) \cdot \delta F_i(t+\tau) \rangle}{\langle F_i(t) \rangle^2}$$

where δF_i is the flunctuation of F_i away from the average value and i is either G or R. The cross-correlation curve was calculated in a similar way, namely:

$$G_X(\tau) = \frac{\langle \delta F_R(t) \cdot \delta F_G(t+\tau) \rangle}{\langle F_R(t) \rangle \cdot \langle F_G(t) \rangle}$$

Prior to fitting the FCS data, individual 15 s autocorrelation curves were averaged together. Any curves showing large amplitude decays with decay times longer than 1 s were assumed to reflect large vesicles or other immobile aggregates and thus were excluded from the data fitting calculation.

The autocorrelation curves were fit to a single-component two-dimensional diffusion model with triplet relaxation:

$$G_i(\tau) = \frac{1}{\langle N_i \rangle} \cdot \frac{1 - F + F e^{-\tau/\tau_T}}{1 - F} \cdot \frac{1}{1 + \tau/\tau_{Di}}$$

where N_i represents the number of diffusing species with fluorophore i (monomers + dimers), F is the fraction of molecules in the triplet state, τ_T is the triplet relaxation time, and τ_{Di} is the dwell time of molecules in the laser focus. The gamma factor typically used to account for the Gaussian shape of the detection volume is assumed to be 1. This cancels out in for the calculation of f_c values but may lead to a slightly lower K_{eq}. The cross-correlation curve showed no sign of triplet relaxation and thus was fit to the following equation:

$$G_X(\tau) = G_X(0) \cdot \frac{1}{1 + \tau/\tau_{DX}}$$

To calculate the concentration of red-labeled monomers (C_R), green-labeled monomers (C_G), and red/green-labeled dimers (C_X), we used parameters from the fit functions and the area of the laser focus in the membrane. The number of red/green-labeled dimers N_X was calculated from[22]

$$N_X = \frac{G_X(0)}{G_R(0) \cdot G_G(0)}$$

The number of red- and green-labeled monomers, N_{Rm} and N_{Gm}, was obtained by subtracting N_X from N_R or N_G, respectively. Concentrations were calculated by dividing the number of monomers or dimers by the corresponding area of the laser focus (0.332 μm^2 for C_R and 0.304 μm^2 for C_G and C_X).

AUTHOR INFORMATION

Corresponding Author

asmith5@uakron.edu

Present Address

[†]Grove City College, 100 Campus Dr., Grove City, PA 16127.

Author Contributions

[‡]W.D.C. and S.M.S. contributed equally.

Notes

The authors declare no competing financial interest.

■ ACKNOWLEDGMENTS

This work was supported, in part, by funding from the National Eye Institute of the National Institutes of Health (grant R01EY008061 (K.P.)). K.P. is John H. Hord Professor of Pharmacology. We would like to thank Jay T. Groves for the Src16 and Src13-GCN4 plasmids.

■ REFERENCES

(1) (a) Khelashvili, G.; Dorff, K.; Shan, J.; Camacho-Artacho, M.; Skrabanek, L.; Vroling, B.; Bouvier, M.; Devi, L. A.; George, S. R.; Javitch, J. A.; Lohse, M. J.; Milligan, G.; Neubig, R. R.; Palczewski, K.; Parmentier, M.; Pin, J.-P.; Vriend, G.; Campagne, F.; Filizola, M. *Bioinformatics* **2010**, *26*, 1804−1805. (b) Lambert, N. A. *Sci. Signaling* **2010**, *3*, pe12. (c) Milligan, G. *Mol. Pharmacol.* **2013**, *84*, 158−169.

(2) Bortolato, A.; Mobarec, J. C.; Provasi, D.; Filizola, M. *Curr. Pharm. Des.* **2009**, *15*, 4017−4025.

(3) (a) Palczewski, K.; Kumasaka, T.; Hori, T.; Behnke, C. A.; Motoshima, H.; Fox, B. A.; Trong, I. L.; Teller, D. C.; Okada, T.; Stenkamp, R. E.; Yamamoto, M.; Miyano, M. *Science* **2000**, *289*, 739−745. (b) Palczewski, K. *J. Biol. Chem.* **2012**, *287*, 1612−1619.

(4) Nickell, S.; Park, P. S.-H.; Baumeister, W.; Palczewski, K. *J. Cell Biol.* **2007**, *177*, 917−925.

(5) (a) Poo, M.-m.; Cone, R. A. *Nature* **1974**, *247*, 438−441. (b) Liebman, P. A.; Entine, G. *Science* **1974**, *185*, 457−459.

(6) (a) Ernst, O. P.; Gramse, V.; Kolbe, M.; Hofmann, K. P.; Heck, M. *Proc. Natl. Acad. Sci. U.S.A.* **2007**, *104*, 10859−10864. (b) Bayburt, T. H.; Vishnivetskiy, S. A.; McLean, M. A.; Morizumi, T.; Huang, C.-c.; Tesmer, J. J. G.; Ernst, O. P.; Sligar, S. G.; Gurevich, V. V. *J. Biol. Chem.* **2011**, *286*, 1420−1428.

(7) (a) Fotiadis, D.; Liang, Y.; Filipek, S.; Saperstein, D. A.; Engel, A.; Palczewski, K. *Nature* **2003**, *421*, 127−128. (b) Jastrzebska, B.; Ringler, P.; Palczewski, K.; Engel, A. *J. Struct. Biol.* **2013**, *182*, 164−172. (c) Mansoor, S. E.; Palczewski, K.; Farrens, D. L. *Proc. Natl. Acad. Sci. U.S.A.* **2006**, *103*, 3060−3065.

(8) Müller, B. K.; Zaychikov, E.; Bräuchle, C.; Lamb, D. C. *Biophys. J.* **2005**, *89*, 3508−3522.

(9) Endres, N. F.; Das, R.; Smith, A. W.; Arkhipov, A.; Kovacs, E.; Huang, Y.; Pelton, J. G.; Shan, Y.; Shaw, D. E.; Wemmer, D. E.; Groves, J. T.; Kuriyan, J. *Cell* **2013**, *152*, 543−556.

(10) Triffo, S. B.; Huang, H. H.; Smith, A. W.; Chou, E. T.; Groves, J. T. *J. Am. Chem. Soc.* **2012**, *134*, 10833−10842.

(11) O'Shea, E. K.; Klemm, J. D.; Kim, P. S.; Alber, T. *Science* **1991**, *254*, 539−44.

(12) Rodgers, W. *Biotechniques* **2002**, *32*, 1044.

(13) Foo, Y. H.; Naredi-Rainer, N.; Lamb, D. C.; Ahmed, S.; Wohland, T. *Biophys. J.* **2012**, *102*, 1174−1183.

(14) (a) Larson, D. R.; Gosse, J. A.; Holowka, D. A.; Baird, B. A.; Webb, W. W. *J. Cell Biol.* **2005**, *171*, 527−536. (b) Sudhaharan, T.; Liu, P.; Foo, Y. H.; Bu, W.; Lim, K. B.; Wohland, T.; Ahmed, S. *J. Biol. Chem.* **2009**, *284*, 13602−13609.

(15) (a) Gambin, Y.; Lopez-Esparza, R.; Reffay, M.; Sierecki, E.; Gov, N. S.; Genest, M.; Hodges, R. S.; Urbach, W. *Proc. Natl. Acad. Sci. U.S.A.* **2006**, *103*, 2098−2102. (b) Saffman, P. G.; Delbruck, M. *Proc. Natl. Acad. Sci. U.S.A.* **1975**, *72*, 3111−3113. (c) Naji, A.; Levine, A. J.; Pincus, P. A. *Biophys. J.* **2007**, *93*, L49−L51. (d) Ly, S.; Bourguet, F.; Fischer, N. O.; Lau, E. Y.; Coleman, M. A.; Laurence, T. A. *Biophys. J.* **2014**, *106*, L05−L08.

(16) Guo, L.; Har, J. Y.; Sankaran, J.; Hong, Y.; Kannan, B.; Wohland, T. *ChemPhysChem* **2008**, *9*, 721−728.

(17) (a) Herrick-Davis, K.; Grinde, E.; Cowan, A.; Mazurkiewicz, J. E. *Mol. Pharmacol.* **2013**, *84*, 630−642. (b) Herrick-Davis, K.; Grinde, E.; Lindsley, T.; Cowan, A.; Mazurkiewicz, J. E. *J. Biol. Chem.* **2012**, *287*, 23604−23614.

(18) Kota, P.; Reeves, P. J.; RajBhandary, U. L.; Khorana, H. G. *Proc. Natl. Acad. Sci. U.S.A.* **2006**, *103*, 3054−3059.

(19) Albertazzi, L.; Arosio, D.; Marchetti, L.; Ricci, F.; Beltram, F. *Photochem. Photobiol.* **2008**, 9999.

(20) Jura, N.; Endres, N. F.; Engel, K.; Deindl, S.; Das, R.; Lamers, M. H.; Wemmer, D. E.; Zhang, X.; Kuriyan, J. *Cell* **2009**, *137*, 1293−1307.

(21) Kasai, R. S.; Suzuki, K. G. N.; Prossnitz, E. R.; Koyama-Honda, I.; Nakada, C.; Fujiwara, T. K.; Kusumi, A. *J. Cell Biol.* **2011**, *192*, 463−480.

(22) Bacia, K.; Kim, S. A.; Schwille, P. *Nat. Methods* **2006**, *3*, 83−89.